ACS Catalysis

Research Article

pubs.acs.org/acscatalysis

Influence of the Reaction Temperature on the Nature of the Active and Deactivating Species during Methanol to Olefins Conversion over H-SSZ-13

E. Borodina,[†] F. Meirer,[†] I. Lezcano-González,[†] M. Mokhtar,[‡] A. M. Asiri,[‡] S. A. Al-Thabaiti,[‡] S. N. Basahel,[‡] J. Ruiz-Martinez,*[,†] and B. M. Weckhuysen*[,†]

[†]Utrecht University, Universiteitsweg 99, Utrecht 3584 CG, The Netherlands

[‡]King Abdulaziz University, P.O. Box 80203, Jeddah 21589, Saudi Arabia

Supporting Information

ABSTRACT: The formation of hydrocarbon species during the methanol to olefins (MTO) reaction over zeolite H-SSZ-13 has been systematically studied at reaction temperatures between 573 and 723 K with a combination of operando UV−vis spectroscopy and online gas chromatography. It was found that the applied reaction temperature influences the rate and nature of coke formation as well as the catalyst stability. Correlation between all hydrocarbon species formed inside the catalyst pores with the activity and deactivation of H-SSZ-13 zeolite material was established. By using a multivariate analysis, we found that the nature of the active and deactivating species varies with the reaction temperature. The majority of active hydrocarbon pool species at low reaction temperatures (i.e., 573−598 K) are methylated benzene carbocations, while at high reaction temperatures (i.e., 623−723 K) methylated naphthalene carbocations become dominant. At low reaction temperatures the deactivation occurs because of the pore filling with methylated naphthalene carbocations. In contrast, at higher reaction temperatures the formation of phenanthrene, pyrene carbocations, and highly conjugated polyaromatics during the deactivation increases. This suggests that the formation of highly conjugated polyaromatics on the external surface can play a role in the deactivation of the material by pore blockage.

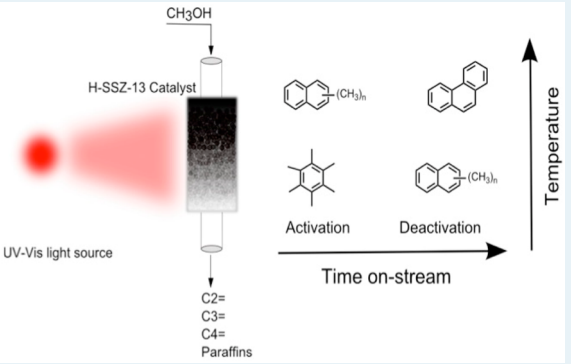

KEYWORDS: *methanol to olefins, UV−vis spectroscopy, in situ spectroscopy, active species, catalyst deactivation*

1. INTRODUCTION

The relatively high price of crude oil and its envisaged shortage in the long run have generated great interest in the development of new catalytic technologies to convert natural gas, coal, or biomass into transportation fuels and chemicals. Alcohol to olefins (ATO) is generally considered as an alternative way to produce gasoline as a transportation fuel, as well as ethylene and propylene as two of the major building blocks for the chemical industry.

Since the 1970s this process has attracted a great deal of interest in both the academic and industrial worlds.[1] During the last four decades a wide range of molecular sieves have been studied in order to find the most suitable methanol to olefins (MTO) catalyst for a specific application.[2] The medium-pore zeolite H-ZSM-5 and the small-pore silicoaluminophosphate H-SAPO-34 are usually applied in methanol to hydrocarbons (MTH) and MTO reactions, respectively. They both contain Brønsted and Lewis acid sites, which are responsible for the catalytic performance.[3] H-ZSM-5 is used to obtain light olefins, aromatics, and paraffins,[4,5] while H-SAPO-34 and its aluminosilicate counterpart H-SSZ-13 and other small-pore zeotypes are mostly applied to the production of light olefins.[6−8]

It is generally considered that the selectivity of H-SAPO-34 and H-SSZ-13 molecular sieves toward ethylene and propylene is related to their CHA topology, which consists of a three-dimensional system with small eight-membered-ring windows with a diameter of 3.8 Å that restrict the diffusion of bulk and branched hydrocarbons.[9] Although both catalysts show sufficient activity and selectivity, their stability is still in need of improvement, as the materials tend to deactivate relatively quickly.[10−13]

One way to study catalyst deactivation is to investigate the material under relevant reaction conditions with spectroscopic and microscopic methods. Several research groups have focused their research interests in the past decade on the study of both reaction and deactivation mechanisms using UV−vis, Raman, IR, and NMR techniques, often in a combined manner.[14−21] For example, UV−vis spectroscopy allows the detection of

Received: September 7, 2014
Revised: December 21, 2014

DOI: 10.1021/cs501345g
ACS Catal. 2015, 5, 992−1003

hydrocarbons with conjugated double bonds and unsaturated carbocations; thus, it is possible to monitor the formation of small amounts of cyclic compounds and polyaromatics.[17−19] From these studies, it became clear that during the ATO process the catalyst materials deactivate rapidly due to the formation of aromatics, i.e., coke compounds and their precursors, in the inner pore system as well as on the outer surface. These compounds block the access of reactants to the active sites as well as the mobility of the reaction products diffusing out of the pores. Information about the nature of these coke species still remains ambiguous.

Since the discovery of the MTO conversion, many reaction mechanisms have been proposed.[2] During the last two decades the hydrocarbon pool (HCP) mechanism has been the most accepted.[6] According to this, polymethylated benzene (PMB) carbocations are the main components of HCP: i.e., hexamethylbenzene carbocations are mostly trapped inside SAPO-34 catalyst. This has been determined by isotopic labeling experiments and analysis of the hydrocarbons inside of the zeolite.[22] The reaction centers are not the Brønsted acid sites alone but inorganic−organic composite including a PMB, which is in interaction with a proton. Methyl groups are added to the pool during the reaction with methanol, followed by splitting off of the olefins.[6,23] Within the HCP mechanism on chabasite-type materials, there are two main reaction mechanisms proposed: paring[24] and side-chain models.[25] On H-SSZ-13, the zeolite with a CHA structure, the active species are believed to be the same. However, there are very limited studies that report a true operando characterization of this zeolite. Recently, H-SSZ-13 has gained interest in the literature, as the introduction of mesopores in these crystals leads to a decrease in the deactivation due to coke formation.[26,27]

In this research work the formation of hydrocarbon species during the MTO reaction over H-SSZ-13 molecular sieves has been systematically studied with a combination of operando UV−vis spectroscopy and online gas chromatography, as outlined in Figure 1.

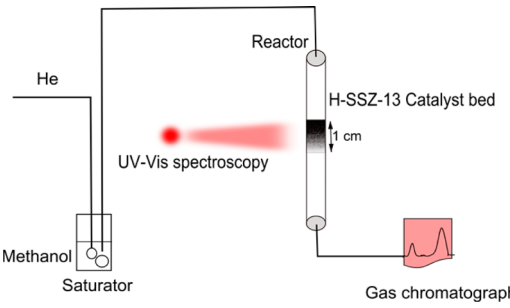

Figure 1. Scheme of the operando UV−vis spectroscopy setup for monitoring the active and deactivating hydrocarbon pool species during the methanol to olefins (MTO) reaction over H-SSZ-13.

This approach gives the opportunity to elucidate the nature of the species, which are formed inside the pore structure of H-SSZ-13 at different stages of the MTO reaction and correlate them with the catalytic performance of the material. We investigated the influence of the reaction temperature on the rate of formation, amount, and nature of the species. With the aid of non-negative matrix factorization (NNMF; see below) of the operando UV−vis spectra it was possible to separate the manifold of hydrocarbon species formed into the two main groups, i.e. species, which are responsible for the activity of the catalyst material and species, related to catalyst deactivation. With these results in hand, we have been able to observe that the nature of the active and deactivating species changes with the reaction temperature, and we provide new insight into the hydrocarbon pool mechanism taking place within H-SSZ-13 catalyst during the MTO process.

2. EXPERIMENTAL SECTION

2.1. Synthesis and Characterization of H-SSZ-13 Zeolite. An Al-containing H-SSZ-13 material was synthesized as described previously, but using static conditions.[28] The sample was calcined in air with the following temperature program: 1 K/min to 393 K, held for 2.5 h; 2.2 K/min to 623 K, held 3 h at this temperature; finally 0.8 K/min to 853 K, held for 3 h. After calcination the sample was in its H-form. The crystal size and morphology were determined by scanning electron microscopy (SEM) using a Tecnai FEI XL 30SFEG instrument. The chemical analysis was performed by inductively coupled plasma optical emission spectrometry (ICP-OES) with a PerkinElmer 3300DV instrument. Purity and identity were verified by a Bruker D2 X-ray powder diffractometer equipped with a Co Kα X-ray tube (λ = 1.7902 Å). X-ray diffraction (XRD) patterns were recorded in the region of 5−50° 2θ at room temperature. The acidity of the samples was measured by temperature-programmed desorption (TPD) with ammonia as probe molecule using a Micrometrics AutoChem 2910 apparatus. Prior to the adsorption of ammonia, 100 g of the sample placed in a quartz tube reactor was preheated at 823 K under 25 mL/min of He flow for 30 min. Adsorption of ammonia (5 vol % in He) was done for 45 min at 373 K. In order to remove physisorbed ammonia, the sample was flushed with a He stream (50 mL/min) at 373 K for 2 h. The ammonia desorption was carried out under a He flow in the temperature range 373−873 K at a heating rate of 10 K/min. The amount of adsorbed ammonia was monitored with a thermal conductivity detector (TCD). Fourier transform infrared (FT-IR) spectroscopy in transmission mode was performed on self-supporting zeolite wafers using a PerkinElmer System 2000 FT-IR spectrometer. The measurements were carried out in the wavenumber range 4000−400 cm^{-1} with 4 cm^{-1} resolution. Prior to the measurements, the samples were preheated in a He flow from 298 to 773 K and held at the final temperature for 2 h to remove water and other impurities adsorbed on the zeolite. CO was supplied from a vacuum line attached to the IR cell, which was kept at 77 K. The pressure of CO added to the cell was in the range 0.03−1 mbar. Pore volumes and BET surface areas were determined by argon adsorption measurements using a Micromeritics ASAP 2420 instrument.

2.2. MTO Reaction over H-SSZ-13 Catalyst Material. Catalytic testing was done in a fixed-bed quartz reactor. The catalyst powder was pressed to give pellets, followed by crushing and sieving. The 212−425 μm fraction was used for catalytic testing. Prior to the reaction ∼50 mg of the catalyst was activated at 823 K under 100% oxygen for 1 h and then cooled to the desired reaction temperature. The weight hourly space velocity (WHSV) of methanol was kept at 0.5 g g^{-1} h^{-1} by flowing He gas through a methanol saturator, which was kept at a temperature of 293 K. The temperature of the reaction was varied between 573 and 723 K. Analysis of the reactant and reaction products was performed with online gas chromatography (GC) by using an Interscience Compact GC instrument equipped with Rtx-1+Rtx-Wax columns and Rt-

DOI: 10.1021/cs501345g
ACS Catal. 2015, 5, 992−1003

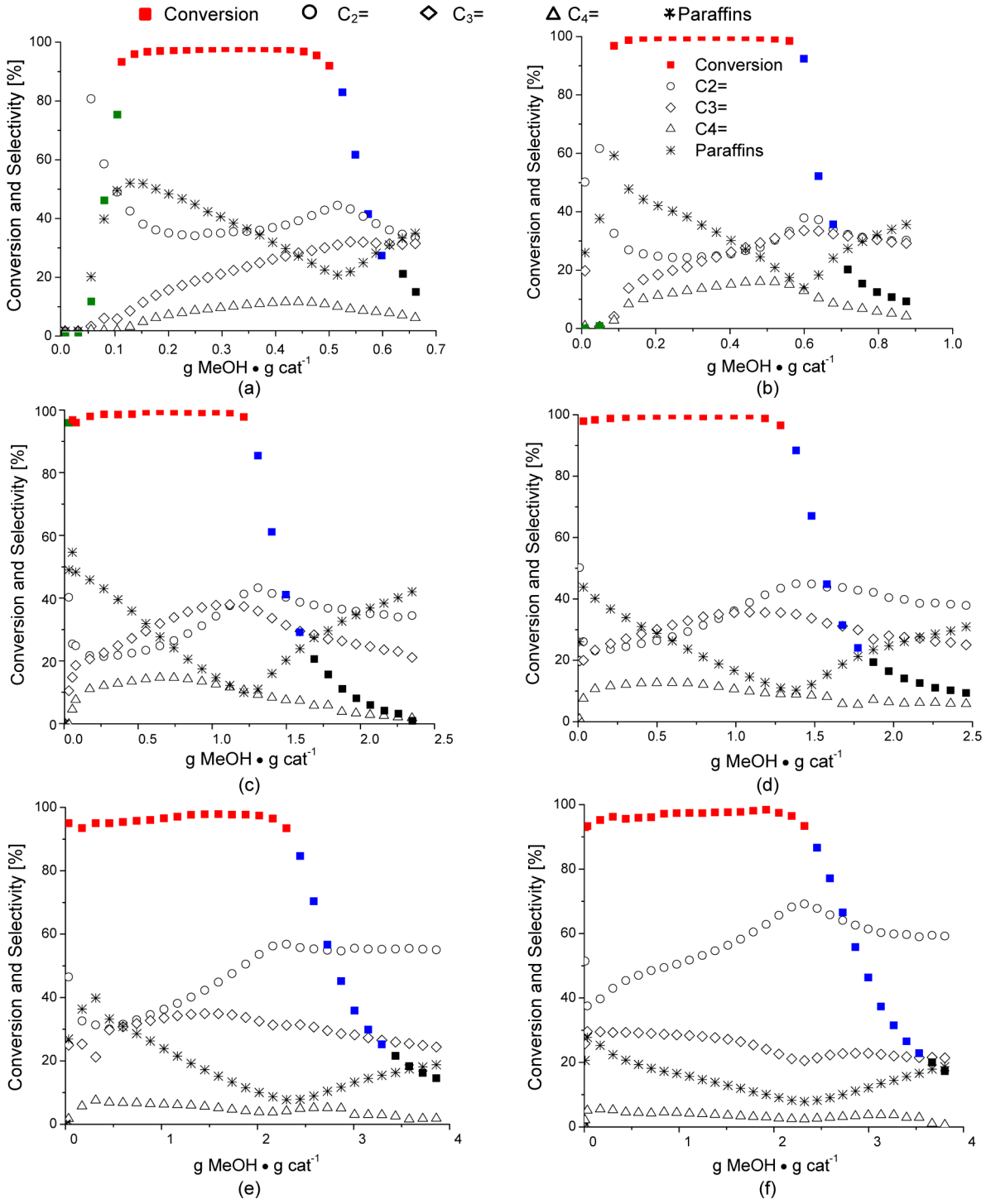

Figure 2. Conversion and selectivity patterns for the MTO reaction as a function of methanol loading on the catalyst material over H-SSZ-13 at a WHSV of 0.5 g g^{-1} h^{-1} for reaction temperatures (a) 573 K, (b) 598 K, (c) 623 K, (d) 648 K, (e) 673 K, and (f) 723 K. The green points correspond to the induction period, when conversion of methanol is less than 100%, the red points indicate a period of full conversion of methanol, the blue points relate to the deactivation period, when the conversion of methanol drops from 100% to 20%, and the black points correspond to the deactivated catalyst, when the conversion of methanol is less than 20%.

TCEP+Rtx-1 and Al_2O_3/Na_2SO_4 columns, respectively, and two flame ionization detectors (FIDs). The olefins/water feeding experiment was carried out in the same manner as the catalytic testing. Instead of methanol, a mixture of ethylene, propylene, and water was flown through the H-SSZ-13 catalyst at 573 K. The WHSVs were 0.3, 0.3, and 2.4 g g^{-1} h^{-1}, which is 17 times more than the amount produced in the MTO reaction at 573 K due to the limitations of the setup mass flow controllers.

2.3. Determination of the Hydrocarbons Retained after the MTO Reaction by Thermogravimetric Analysis (TGA). The amount of organic compounds retained after the MTO reaction over the catalyst was determined by thermogravimetric analysis. A 10−15 mg portion of the spent

DOI: 10.1021/cs501345g
ACS Catal. 2015, 5, 992−1003

catalyst was heated in O_2 (flow rate 10 mL/min) from 323 to 1173 K (ramp 10 K/min) and held at 1173 K for 60 min. The analysis was done using PerkinElmer Pyris 1 TGA combined with an MS detector.

2.4. Operando UV−Vis Spectroscopy of the MTO Reaction over H-SSZ-13 Catalyst Combined with NNMF. The hydrocarbon pool active species and related coke compounds formed during the MTO processes were determined using operando UV−vis spectroscopy. The measurements were performed in the wavenumber range of 11000−50000 cm^{-1} using a high-temperature UV−vis probe provided by Avantes. The probe comprises one excitation and one collection optical fiber with a size diameter of 400 μm and length of 1.5 m, which are placed in a stainless steel protection sleeve. The probe was connected to a deuterium−halogen light source and an AvaSpec 2048 UV−vis spectrometer. The probe was custom-made to operate at temperatures up to 873 K. The spectra were saved every 20 s, with 100 accumulations of 140 ms exposure time each.

NNMF was applied to the UV−vis spectra. NNMF[29,30] is a widely used factor analysis method to factorize a (non-negative) data matrix $T \times W$ into two matrices X $(T \times k)$ and Y $(k \times W)$ with the constraints that all matrices have only positive elements. Here, the data matrix represents the data stack consisting of hundreds of single UV−vis spectra with wavenumber W collected at different times T. This factorization is typically not exactly solvable and therefore is approximated numerically; the result X^*Y (of rank k) is a lower rank approximation to the data matrix, and the rows of $k \times W$ are the so-called eigenspectra of the data. The factors X and Y can be calculated by minimizing the root-mean-squared residual between the data matrix and X^*Y, using an alternative least-squares (ALS) algorithm or a multiplicative update algorithm.[30,31] In this work NNMF was performed using the ALS algorithm with a minimum number of 500000 iterations and a two-rank approximation ($k = 2$), effectively deconvoluting the data into two groups with different kinetics, where each group pools spectral bands with similar kinetics.

2.5. Determination of the Hydrocarbons Retained after the MTO Reaction by Gas Chromatography−Mass Spectrometry (GC-MS). The composition of retained hydrocarbons in the spent catalyst after quenched and full MTO reactions was analyzed by GC-MS. Prior to the analysis, the catalyst was flushed with He and cooled to 343 K. During this process, UV−vis spectra were continuously collected in order to monitor potential changes in the chemistry of the species during the quenching procedure.

A 15 mg portion of the spent catalyst was transferred to a Teflon tube and dissolved in 1.0 cm^3 of 48% HF for 30 min. Afterward, 1 cm^3 of CH_2Cl_2 was added to the Teflon tube and the mixture was shaken for 30 min. The water and organic phases were left to separate for 30 min. The extraction was repeated three times. A 1 μL portion of the resulting organic solution was analyzed by a GCMS-QP2010 instrument (Shimadzu) connected to a MS detector.

3. RESULTS AND DISCUSSION

3.1. Catalyst Characterization. The XRD pattern of the calcined H-SSZ-13 catalyst, shown in Figure S1a in the Supporting Information, confirms that CHA is the crystalline phase in the zeolite material under investigation. The crystal size of the material, as determined by SEM and illustrated in Figure S1b,c in the Supporting Information, is ∼1−10 μm. The Si/Al ratio determined by elemental analysis, as measured by ICP-AES, is 15. This corresponds to 2.1 acid sites per cage, theoretically. In order to determine the acidic properties of the H-SSZ-13 material, TPD measurements with ammonia as probe molecule were determined and the results are shown in Figure S1d in the Supporting Information. The H-SSZ-13 zeolite sample has both strong and weak acid sites, which correspond respectively to the TPD peaks at low (428 K) and high temperatures (718 K).[32,33] It was determined that 81% of aluminum atoms replace silicon in the structure, thereby creating Brønsted acid sites. The acid strength was also calculated by CO adsorption followed by FT-IR spectroscopy (Figure S2 in the Supporting Information).[11,34] The adsorption of CO on the dehydrated H-SSZ-13 sample leads to a red shift of the two types of Brønsted acid sites ($\Delta\nu_{OH}$ = 316 cm^{-1}). When all OH groups are occupied with CO molecules, a band of physisorbed CO at ∼2139 cm^{-1} is detected ($\Delta\nu_{CO}$ = +35 cm^{-1}). The magnitude of the shifts is proportional to the strength of the Brønsted acid sites. This result correlates with the literature data obtained for H-SSZ-13 molecular sieves.[11,34] Ar adsorption and desorption isotherms are shown in Figure S3 in the Supporting Information. The material has a BET surface area of 700 m^2/g and is fully microporous, with a pore volume of 0.24 cm^3/g; similar results have been reported in the literature.[28,32,34] A more in-depth discussion about the catalyst characterization can be found in the Supporting Information.

3.2. Catalytic Performance. In a first set of experiments we evaluated the catalytic performance of H-SSZ-13 as a function of reaction temperature (i.e., 573, 598, 623, 648, 673, and 723 K) using a weight hourly space velocity (WHSV) of 0.5 g g^{-1} h^{-1}. The activity data, expressed as methanol conversion vs methanol throughput on the catalyst material and selectivity patterns, are summarized in Figure 2. Figure 2 shows that the reaction temperature influences the catalyst lifetime, which increases with temperature. However, there is not a significant difference in catalyst lifetime for reaction temperatures between 573 and 598 K, while for temperatures of 623 and 648 K an increase in catalyst stability was observed. A further rise of the reaction temperature up to 673−723 K corresponds to a higher amount of converted methanol per gram of catalyst material. The catalytic performance of H-SSZ-13 with the reaction temperature was previously discussed by Bleken et al.[11] In that work, temperatures of 623 and 648 K were reported as optimum for methanol conversion. Under our studied conditions, the highest catalytic lifetime was reached at 673 and 723 K. The differences in catalytic stability are dependent on the reaction temperature. For all tested reaction temperatures the selectivity toward paraffins is over 30% at the beginning of the reaction and decreases with time on stream and the reaction temperature. The reason for this is most probably the high acidity of H-SSZ-13, which favors hydride transfer reactions and therefore the formation of byproducts, such as C_1−C_5 paraffins and aromatics.[35−37]

These side reactions become less important with the progress of the reaction and the temperature.[10] Furthermore, the low selectivity toward propylene, observed at the beginning of the reaction, can be also related to its interconversion to form active aromatic hydrocarbon pool species.[38] The CHA structure consists of cages connected by small eight-membered-ring windows, so that only C_1−C_5 hydrocarbons can diffuse through the catalyst pores. Generally, the product range mostly consists of C_2 and C_3 olefins, with smaller amounts of C_4 products and some traces of C_5 hydrocarbons. As shown in Figure 2, the

DOI: 10.1021/cs501345g
ACS Catal. 2015, 5, 992−1003

selectivity patterns are typical for the CHA structure of the catalyst.[39] The selectivity toward ethylene and propylene increases with time on stream. The deactivation period is accompanied by a selectivity decrease toward low olefins and a selectivity increase toward paraffins.

3.3. Determination of the Amount of Retained Hydrocarbons on H-SSZ-13 Catalyst Material in the MTO Reaction. In order to determine the amount of retained hydrocarbons with reaction temperature, a thermogravimetric analysis of the spent H-SSZ-13 samples in oxygen has been performed. We define spent catalyst as the material after complete deactivation, i.e., the material taken from the reactor just after performing the catalytic tests plotted in Figure 2. This means that the time that the spent catalyst has been on stream depends on the exact reaction temperature.

The data are summarized in Figure 3. The TGA measurements show that the total coke content differs only slightly for

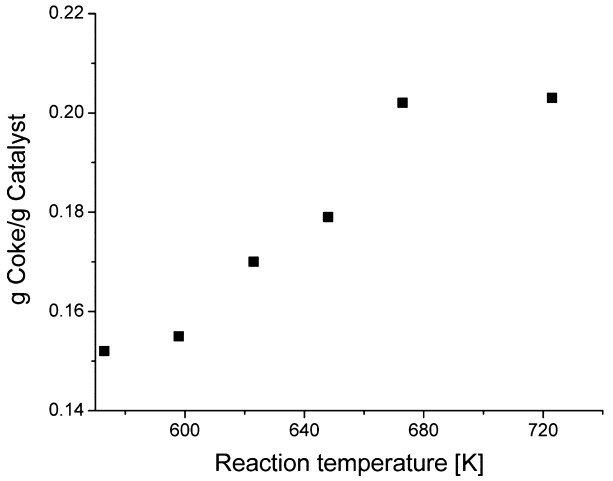

Figure 3. Coke content of the spent zeolite catalyst material at different reaction temperatures.

the reactions carried out at 573 and 598 K. The values are ~0.15 g of coke/g of H-SSZ-13 catalyst. An increase in the reaction temperature up to 673 K leads to a linear increase in the amount of retained hydrocarbons up to 0.20 g/g of catalyst. At this point the total amount of coke is independent of further increases in reaction temperature up to 723 K.

The fact that the amount of coke increases with the reaction temperatures in the range of 598−673 K can be explained by a more efficient use of the material. In particular, these results are in line with the catalytic stability of H-SSZ-13 catalyst material, where the highest stability is obtained at reaction temperatures of 673 and 723 K (Figure 2). The observation of the temperature-dependent formation of coke is, however, in contrast to the literature, as it has been reported that the final amount of coke was independent of temperature.[11] The differences can be due to the fact that other parameters, such as space velocity and particle size, can affect the formation of coke. We have investigated the effect of WHSV (0.5, 1, and 3 g g^{-1} h^{-1}), and it does not affect the amount of coke. Therefore, these changes can be attributed to the differences in crystal size. The large crystals utilized in this work (2−8 μm) are less efficiently used at low reaction temperatures in comparison to small crystals (0.2−2 μm).[11] A higher reaction temperature favors the efficient use of the crystals and therefore more coke is formed.

3.4. Operando UV−Vis Spectroscopy Measurements. *3.4.1. UV−Vis Spectroscopy.* The H-SSZ-13 catalyst was continuously monitored by operando UV−vis spectroscopy in order to obtain detailed insight into the hydrocarbons formed inside the pores during the MTO reaction. As depicted in Figure 4, different colors have been used to indicate distinct stages in the reaction. Green spectra represent the induction period, red indicates the full conversion of methanol, blue stands for the deactivation period, and black corresponds to the deactivated catalyst.

First, for all reaction temperatures an induction period is observed. The UV−vis spectra for the induction period are shown in Figure S4 of the Supporting Information. We define the induction period as the time until a full conversion of methanol is reached. The induction period is associated with a buildup of the hydrocarbon pool species inside the catalyst cages.[6] Additionally, monitoring the H-SSZ-13 zeolite during the reaction with operando UV−vis spectroscopy allows us to detect the formation of hydrocarbon pool species and their precursors. Both the induction period and the time of the first UV−vis band in the spectra decrease with the reaction temperature, as observed in Table S1 of the Supporting Information.

From the time-resolved spectra during the induction period, two main bands at ~33650 and ~26000 cm^{-1} are observed in the whole range of reaction temperatures. There is a first band appearing at ~33650 cm^{-1}, which is ascribed to monoenyl carbocations.[40,41] These species most likely originate from the protonation and subsequent hydride transfer of olefins on Brønsted acid sites. Other species can contribute to this band, for instance, as suggested by Jentoft et al.,[41] cyclopentenyl carbocations, which are intermediates in the paring mechanism for the formation of olefins.[42] Then another band is observed at ~26000 cm^{-1} due to methylated benzene carbocations,[43−46] which are believed to be the main active species in the formation of olefins for these types of chabazite-like materials.[1,22,42,47−50] The appearance of spectroscopic signatures from olefins prior to the formation of active methylated benzene carbocations suggests that such monoenyl carbocations are most likely formed from the presence of impurities in the methanol feed, as previously suggested by Haw et al.,[50] and/or from the impurities remaining upon the calcination process.

When the catalyst is at full conversion, there is an evolution of the UV−vis spectra (Figure 4). The band ascribed to monoenyl carbocations decreases in intensity, and a new band starts to grow at ~30000 cm^{-1}, which can be ascribed to dienyl carbocations[12,40] and/or benzene carbocations with a low degree of methylation. The reaction temperature affects the dynamics of these bands, which evolves faster when the temperature increases. This indicates that monoenyl carbocations react with olefins to form more conjugated species, such as dienyl and aromatic carbocations with different numbers of benzene rings. With time on stream other bands appear at ~36400, 25400, and 16700 cm^{-1} generated by neutral aromatics,[12,43] neutral polyaromatics,[51−53] and polyaromatic carbocations,[45,46,54] respectively.

In order to understand to a greater extent the origin of the UV−vis bands, an experiment was performed where a mixture of ethylene, propylene, and water was fed to the H-SSZ-13 sample in order to mimic the product stream during the MTO conversion. The ethylene, propylene, and water composition is similar to that detected in the product outlet for the MTO

DOI: 10.1021/cs501345g
ACS Catal. 2015, 5, 992−1003

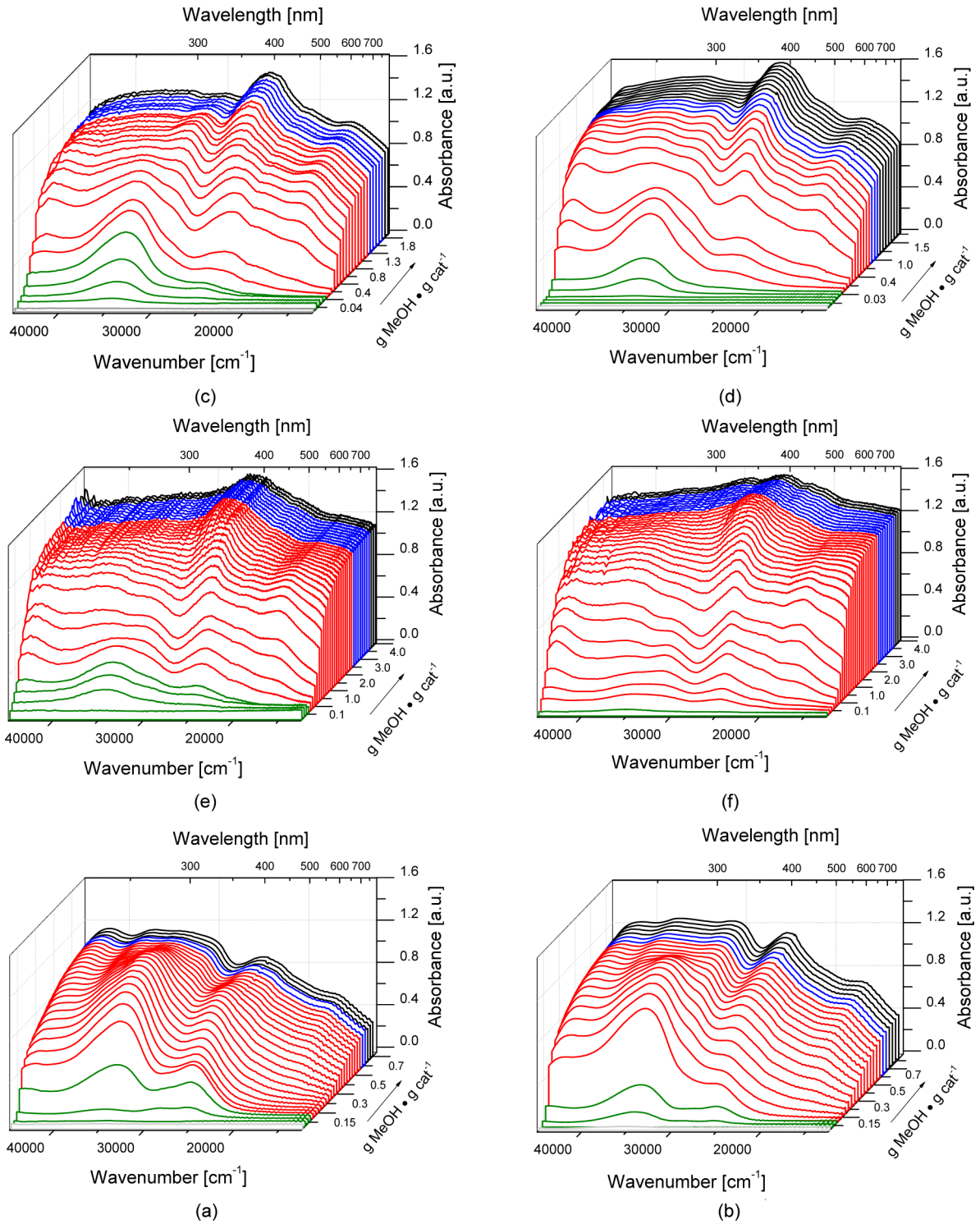

Figure 4. Operando UV−vis spectra recorded for the MTO reaction as a function of methanol loading on the catalyst material over H-SSZ-13 at a WHSV of 0.5 g g^{-1} h^{-1} for reaction temperatures (a) 573 K, (b) 598 K, (c) 623 K, (d) 648 K, (e) 673 K, and (f) 723 K. The green spectra correspond to the induction period, when conversion of methanol is less than 100%;, the red spectra indicate a period of full conversion of methanol, the blue spectra relate to the deactivation period, when the conversion of methanol drops from 100% to 20%, and the black spectra correspond to the deactivated catalyst, when the conversion of methanol is less than 20%.

reaction at 100% conversion and at 573 K. The H-SSZ-13 zeolite was pretreated in the same way as for the MTO reaction described in the Experimental Section. The composition of the gas outlet and operando UV−vis spectra of the catalyst are plotted in Figure 5.

The results of the gas outlet composition show that both ethylene and propylene are converted into the products, trapped inside the catalyst. The operando UV−vis results display all the bands observed in the MTO reaction with the exception of the 26000 cm^{-1} band, ascribed to highly methylated benzene carbocations.[45,46] We call benzene

DOI: 10.1021/cs501345g
ACS Catal. 2015, 5, 992−1003

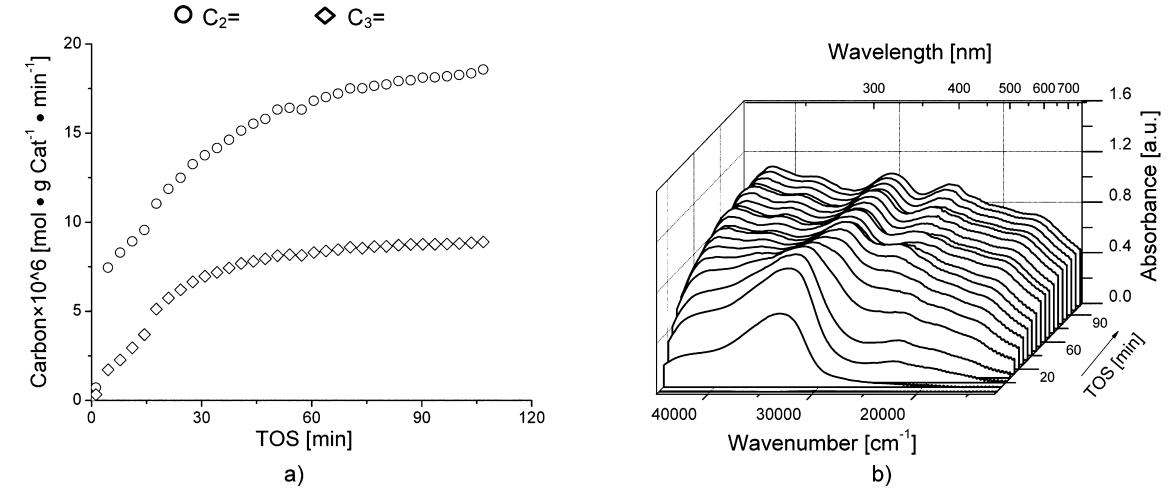

Figure 5. (a) Composition of the gas outlet detected in the effluent and (b) corresponding operando UV−vis spectra collected during feeding of a mixture of ethylene, propylene, and water as a function of time over H-SSZ-13 at 573 K. The composition of the gas outlet and spectra were plotted every 3 min.

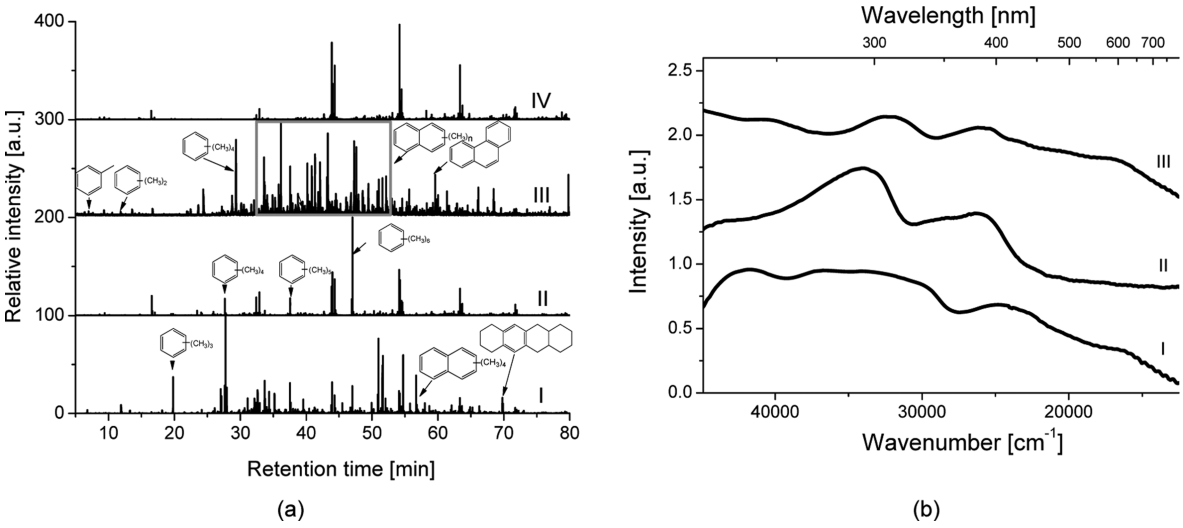

Figure 6. (a) Gas chromatograms of the retained hydrocarbons and (b) corresponding stacked UV−vis spectra in H-SSZ-13: (I) after the MTO reaction at 573 K; (II) quenched MTO reaction after flowing 0.1 g MeOH/g of catalyst at 573 K; (III) after feeding a mixture of ethylene, propylene, and water; (IV) blank sample.

carbocations with five to six methyl groups highly methylated, while low methylated stands for benzene carbocations with up to four methyl groups. The fact that we do not observe the band for highly methylated benzene carbocations in the UV−vis spectra collected during feeding the mixture of ethylene, propylene, and water means that such a band can only be formed when methanol is used as a reagent. Indeed, only the band at ∼24500 cm^{-1} is observed. We applied a NNMF analysis to this set of spectra to verify the absence of highly methylated benzene carbocations. The analysis will be explained in detail below.

3.4.2. Nature of the UV−Vis Absorption Bands. For a more accurate assignment of the UV−vis bands, we combined those experiments with gas chromatography−mass spectrometry (GC-MS) analysis of the hydrocarbons trapped in the H-SSZ-13 catalyst by a dissolution−extraction method previously reported.[11] UV−vis spectra of the spent catalyst were collected in order to monitor potential changes in the chemistry of the species. The UV−vis spectra at different reaction temperatures (i.e. 573−773 K) show a few changes after the cooling process. Mainly, some of the bands shift to lower wavenumbers. Importantly, the band at 30000 cm^{-1}, ascribed to low methylated benzene carbocations, red shifts around 800 cm^{-1}, which is in the range that we reported (29000−31000 cm^{-1}). This shows that temperature might affect the exact position of the absorption bands. The spectra of the samples after deactivation and out of the reactor are shown in Figure S5 in the Supporting Information. However, that is not the case for the quenched MTO reaction at 573 K. For this purpose, first we show in Figure 6 the chromatograms and corresponding UV−vis spectra of the quenched reaction (after flowing 0.1 g of MeOH/g of catalyst) and at end of the MTO reaction at 573 K.

The chromatogram of the quenched reaction shows three main components, which are tetramethyl-, pentamethyl-, and hexamethylbenzenes, the last being the most abundant. The UV−vis results show the two main contributions at ∼33650 and ∼26000 cm^{-1}, with a shoulder at ∼29000 cm^{-1}. Considering that monoenyl carbocations do not have an aromatic nature and they are most likely gas phase products that are not analyzed, the band at ∼26000 cm^{-1} can be

DOI: 10.1021/cs501345g
ACS Catal. 2015, 5, 992−1003

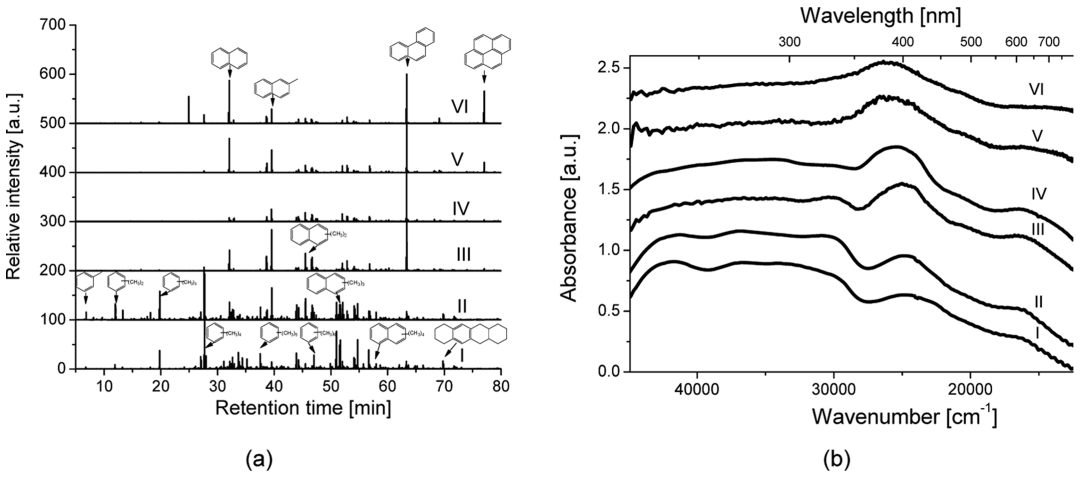

Figure 7. (a) Gas chromatograms of the retained hydrocarbons and (b) corresponding stacked UV−vis spectra in H-SSZ-13 after the MTO reaction at (I) 573 K, (II) 598 K, (III) 623 K, (IV) 648 K, (V) 673 K, and (VI) 723 K.

attributed to highly methylated benzene (penta and hexa) carbocations, whereas the shoulder at ∼29000 cm^{-1} can be ascribed either to dienyl[40,55,56] or to less methylated aromatics, such as tri- and tetramethylbenzene carbocations. Moreover, the chromatogram of the retained hydrocarbons after feeding the mixture of olefins and water does not show hexamethylbenzene and the band at ∼26000 cm^{-1} is not present on the corresponding UV−vis spectrum. Therefore, this confirms the correct assignment of the latter band to highly methylated benzene carbocations and supports our suggestion that they can be formed only when methanol is used as a reagent.

The chromatogram of the sample after full reaction at 573 K displays two main contributions of bicyclic methylated aromatics, such as trimethyl- and tetramethylnaphthalenes, and low methylated benzenes with a contribution of penta- and hexamethylbenzenes. From the UV−vis spectrum at the end of the reaction, the broad band at ∼25200 cm^{-1} and the shoulder at ∼24000 cm^{-1} can be attributed to highly methylated benzene (penta- and hexamethylbenzenes) and methylated naphthalene carbocations, respectively. It is worth noting that the shoulder at ∼29000 cm^{-1} was developed during the cooling down of H-SSZ-13 (Figure S6 in the Supporting Information), which is due to the demethylation of highly methylated benzenes into tri- and tetra-methylbenzenes. Our findings suggest that the band at ∼29000 cm^{-1} corresponds to low methylated benzene carbocations. However, the proposal is not in agreement with previous studies by Bjørgen et al.,[44] where polymethylbenzenes carbocations with less than four methyl groups may not be protonated in H-Beta zeolite at 300 K. This disagreement could be due to the different temperatures applied, since our experiments were conducted in the temperature range 573−723 K. Moreover, Bjørgen et al. observed the absorbance of tetramethylbenzene carbocations at ∼26500 cm^{-1}, but according to our results the position of the band for tri- and tetramethylbenzene carbocations shifts to ∼29000 cm^{-1}. This is also proven by our experiments when the catalyst is cooled to 598 K, in which we could observe a red shift (around 800 cm^{-1}) of the band at ∼29000 cm^{-1} when the catalyst was at room temperature. Differences in the position of the band can be also affected by zeolite topology. Bjørgen et al. performed the adsorption of tetramethylbenzene on H-Beta and we used SSZ-13 zeolite. This effect of the zeolite topology on the position of the UV−vis absorption bands has been previously reported by Hemelsoet et al.[46] by using time-dependent density functional theory calculations. The geometrical relaxation of benzene species is limited and can only account for a maximum shift of around 1200 cm^{-1}. Considering all these effects, we are closer to the data reported by Bjørgen and co-workers.

The chromatograms corresponding to the UV−vis spectra for the higher temperature experiments are represented in Figure 7.

The increase in the reaction temperature leads to the formation of different compounds. For example, at 598 K, less methylated benzenes appear at the expense of highly methylated benzenes. For even higher temperatures, no more monoaromatics are observed and the composition shifts from highly methylated naphthalenes to low methylated naphthalenes. Finally, at the highest temperatures (673 and 723 K), more conjugated polyaromatics appear, such as phenanthrene and pyrene. These results show that naphthalene and methylnaphthalene carbocations give rise to a band at ∼24000 cm^{-1}, which can overlap with the contribution of highly methylated benzene carbocations. Additionally, the band at ∼16700 cm^{-1} seems to be related to the formation of polyaromatic carbocations, such as phenanthrene, and the shoulder at shorter wavenumbers to even more conjugated systems such as pyrene carbocations. The assignments of the bands are summarized in Table 1.

3.4.3. Active and Deactivating Species As Determined by Operando UV−Vis Spectroscopy and NNMF Analysis. After the assignment of the operando UV−vis bands to distinct hydrocarbon species, we aimed to understand in more detail the role of those species in the MTO reaction. Due to the complexity of the spectra and the dynamics of the species during the catalytic process, a multivariate method, called NNMF, was applied to the analysis of the data.

The results of this methodology for the MTO reaction at 573 and 723 K, depicted in Figure 8, show that the operando UV−vis spectra can be broken down into two groups of spectra with different kinetic behavior. This observation can be made for all reaction temperatures (Figures S7 and S8 of the Supporting Information).

The first group of species at 573 K contains absorption bands at ∼33650 and ∼26000 cm^{-1} (Figure 8a), ascribed to monoenyl and highly methylated benzene carbocations, respectively. The dynamics of this group of hydrocarbon

DOI: 10.1021/cs501345g
ACS Catal. 2015, 5, 992−1003

Table 1. Assignments of the Characteristic UV−Vis Bands Observed on H-SSZ-13 during the Methanol to Olefins (MTO) Reaction

species	UV−vis band (cm^{-1})	ref
neutral benzenes	36000−37000	12, 43
monoenyl carbocations	33000−34000	40, 41
alkyl-substituted cyclopentenyl carbocations	33000−34000	41
dienyl carbocations	29000−31000	12, 40, 55, 56
low methylated benzene carbocations (up to four $-CH_3$ groups)	29000−31000	this work
highly methylated benzene carbocations (containing five to six $-CH_3$ groups)	25000−26000	43−46
		this work
methylated naphthalene carbocations	23000−24000	45, 46
		this work
neutral polyaromatics	23000−24000	51−53
phenanthrene/anthracene carbocations	16000−17000	45, 46, 54
		this work

species, displayed in Figure 8b, are strongly linked with the activity of the material and increase with the conversion until reaching a maximum at full conversion. Then the contribution of those hydrocarbon species to the overall operando UV−vis spectra declines with time on stream. The monoenyl carbocations can be formed by side reactions of the olefins, as previously demonstrated with the olefin/water experiment. They are formed when the catalyst is at full conversion but are not considered active species, which are responsible for catalyst activity. However, the highly methylated benzene carbocations are only created by methanol. These results point out that they are the real active species at this reaction temperature. We call it the active species group because it encloses the active species in the reaction and other species, which are related to the formation of olefins but are not directly related to the deactivation of the catalyst.

The second group of hydrocarbon species encloses the bands at ∼30000, 24000, and 17000 cm^{-1}, which are related to low methylated benzene, methylated naphthalene, and phenanthrene carbocations. Their dynamics starts at the maximum formation of the first group of hydrocarbon species and increases until the catalyst is completely deactivated. These results point out that these are the hydrocarbon species formed during the deactivation process and most likely are the cause of deactivation. However, naphthalene and phenanthrene carbocations would be the cause of deactivation, whereas the low methylated benzene carbocations can be formed as a consequence of deactivation.

Interestingly, the reaction temperature strongly affects the nature of both groups of species. For instance, if we look at the MTO reaction at high temperature (723 K), displayed in Figure 8c, two new groups of spectra arise. In the first group the band at ∼26000 cm^{-1} is absent and a new band appears at ∼23000 cm^{-1}, which can be ascribed to highly methylated naphthalene carbocations. Additionally, two other absorption bands at ∼31000 and 17000 cm^{-1}, which might correspond to low methylated benzene and phenanthrene carbocations, appear. This indicates that the nature of the active species depends on the reaction temperature. More specifically, methylated naphthalene carbocations are the real active species at high reaction temperatures. The fact that phenanthrene carbocations appear in the same group of species does not mean that they are responsible for the catalyst activity and they are most likely formed by the side reactions of olefins. The formation of phenanthrene carbocations at high reaction temperatures occurs in the same manner as for monoenyl carbocations at low reaction temperatures.

The same variation of the nature of species applies to the second group, where now a featureless spectrum is encountered, which could be due to the formation of highly conjugated neutral polyaromatics deposited on the external surface of the H-SSZ-13 material. The contribution of the external conjugated polyaromatics increases with reaction temperature. This hinders the identification of the different absorption bands in the operando UV−vis spectra corresponding to individual groups of species, located inside of the pores of the catalyst. Therefore, conjugated polyaromatics play a key role in the deactivation at high reaction temperatures. However, we cannot rule out the effect of phenanthrene and pyrene carbocations as species affecting the deactivation. Indeed, these species were detected as the most abundant retained compounds (Figure 8a) after deactivation of the catalyst. Summarizing, in Table 2 we present the two groups of active and deactivating species as revealed by our operando UV−vis spectroscopy and GC-MS analysis.

The results highlight the dynamics of the organic species inside the catalyst with increasing time on stream and the effect of the reaction temperature in the active and deactivating species during the MTO conversion.

The evolution of the two groups of hydrocarbon species can be explained by the delayed breakthrough behavior of the MTO reaction. Considering that we monitor the whole catalyst bed during the reaction, the spectroscopic data from the deactivating species can be translated as the formation of those species along the catalyst bed. The group of active hydrocarbon species do not exhibit the breakthrough behavior of the conversion, and it seems that there are more active species than are required for full conversion of methanol. The amount, however, decreases with time on stream until the level of active species is not sufficient to ensure full conversion of methanol, and at this moment the catalyst starts to deactivate.

The same methodology has been applied to the absorption spectra collected during the olefins/water feeding experiment in order to verify that highly methylated benzenes are absent during this experiment. The results of the NNMF treatment of the operando UV−vis spectra are shown in Figure 9, where the left part indicates the two groups of hydrocarbon species (Figure 9a) and the right part shows the evolution of every group of species as a function of time (Figure 9b).

It can be seen in Figure 9b, in the beginning of the olefins/water feeding experiment, that enyl carbocations (∼33000 and ∼23000 cm^{-1}) are formed. With time on stream aromatization of those species takes place and the contribution of the second group prevail. As the result shows, the spectral contribution has maxima at ∼29000 and ∼24500 cm^{-1}. The band at ∼29000 cm^{-1} is assigned to the low methylated benzene carbocations and the band at ∼24500 cm^{-1} to methylated naphthalene carbocations rather than penta- and hexamethylbenzenes, which absorb at longer wavenumbers (∼25000−26000 cm^{-1}). As mentioned in section 3.4.2, we do not detect penta- and hexamethylbenzenes in the retained material, while significant amounts of low methylated benzene carbocations and

DOI: 10.1021/cs501345g
ACS Catal. 2015, 5, 992−1003

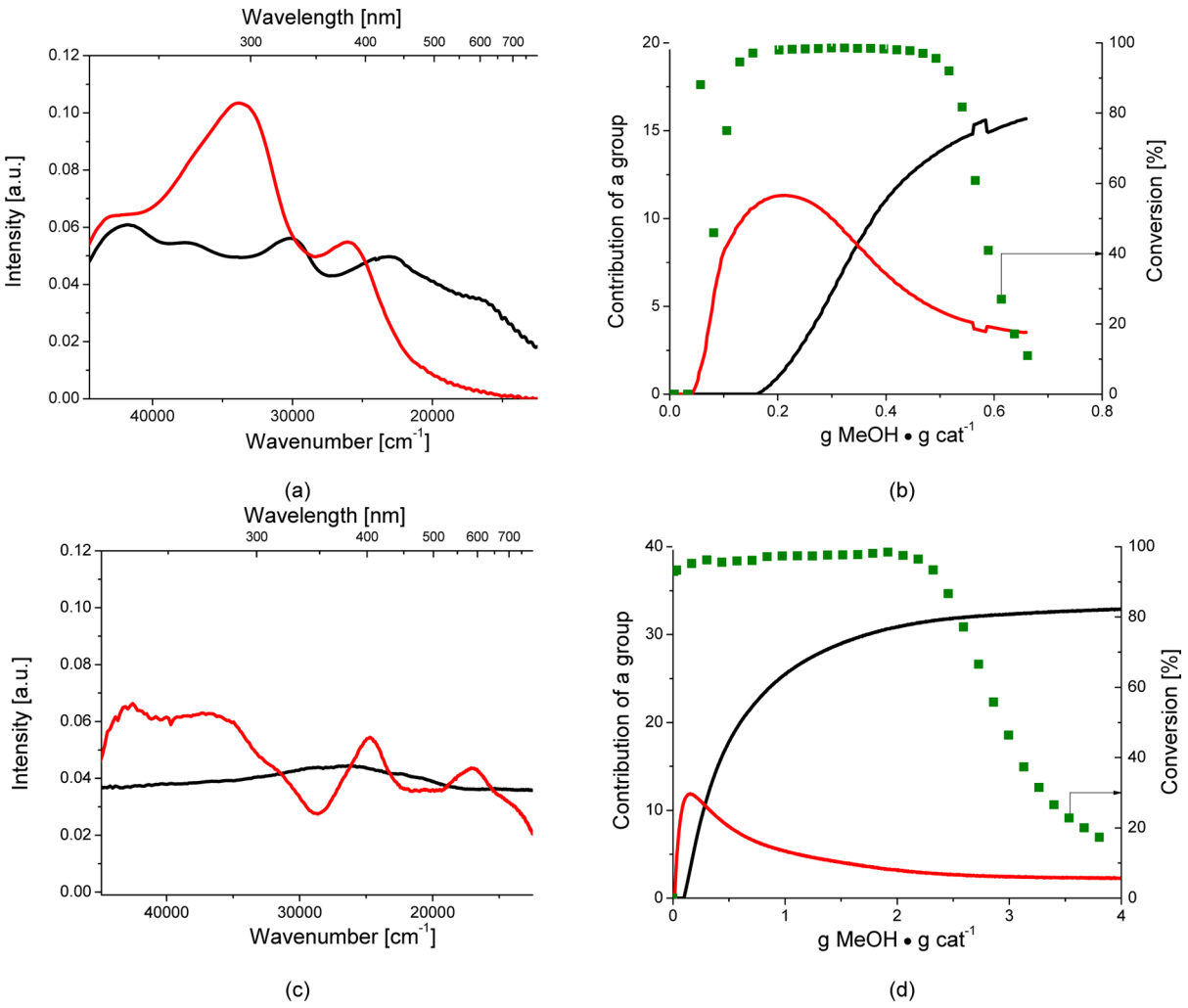

Figure 8. Deconvolution of the operando UV−vis spectra of H-SSZ-13 into two groups of bands (eigenspectra) for the hydrocarbon species with different kinetics (a, c) and the evolution of every group of hydrocarbon species as a function of methanol loading on the catalyst material (b, d), calculated by the NNMF method. The spectra are recorded during the MTO reaction at 573 K (a, b) and 723 K (c, d). The red curve represents group I (active hydrocarbon species), and the black curve corresponds to group II (deactivating hydrocarbon species). The green dots correspond to conversion.

Table 2. Active and Deactivating Hydrocarbon Species Formed during Methanol to Olefins Reactions over H-SSZ-13 at Different Reaction Temperature As Determined by Operando UV−Vis Spectroscopy and GC-MS Analysis of Retained Hydrocarbons

T (K)	active species	deactivating species
573	highly methylated benzene carbocations	methylated naphthalene/phenanthrene carbocations
598	highly methylated benzene carbocations	methylated naphthalene/phenanthrene carbocations
623	highly methylated naphthalene carbocations	phenanthrene carbocations/external conjugated polyaromatics
648	highly methylated naphthalene carbocations	phenanthrene carbocations/external conjugated polyaromatics
673	highly methylated naphthalene carbocations	phenanthrene carbocations/pyrene carbocations/external conjugated polyaromatics
723	highly methylated naphthalene carbocations	phenanthrene carbocations/pyrene carbocations/external conjugated polyaromatics

methylated naphthalene carbocations are observed in the chromatogram of the retained material. The correlation of the positions of the absorption bands formed during olefins/water feeding experiments confirms that highly methylated benzene carbocations are not formed without methanol present in the system.

4. CONCLUSIONS

The catalytic performance and the hydrocarbon species formed within H-SSZ-13 during the MTO reaction has been investigated with operando UV−vis spectroscopy. Within the range of temperatures studied, the catalyst stability increases and the induction period decreases with increasing reaction temperature. The combination of operando UV−vis spectroscopy, dissolution−extraction experiments, and NNMF analysis allowed us to understand the chemistry, dynamics, and role of hydrocarbon species trapped in the cages of H-SSZ-13. In this way, the hydrocarbon species responsible for the activity and deactivation of the catalyst material were identified. Interestingly, the role of those hydrocarbon species changes with reaction temperature. More specifically, the majority of the active hydrocarbon pool species at low reaction temperatures (573 and 598 K) are methylated benzene carbocations, while methylated naphthalene carbocations are determined as the dominant active HCP species at high reaction temperatures (623−723 K). Furthermore, at low reaction temperatures

DOI: 10.1021/cs501345g
ACS Catal. 2015, 5, 992−1003

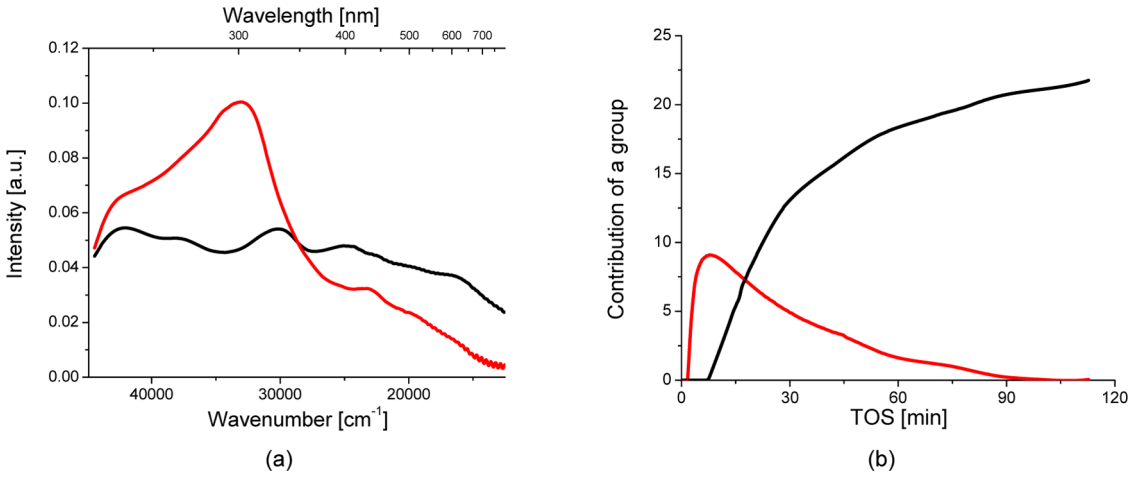

Figure 9. Deconvolution of the operando UV−vis spectra of H-SSZ-13 into two groups of hydrocarbon species (a) and the evolution of every group of hydrocarbon species as a function of time (b), calculated by the NNMF method. The original spectra were recorded during the ethylene, propylene, and water feeding experiment as a function of time over H-SSZ-13 at 573 K.

deactivation occurs because of the pore filling with methylated naphthalene carbocations and, when the reaction temperature is higher, the deactivation is related to phenanthrene and pyrene external conjugated polyaromatics.

■ ASSOCIATED CONTENT

Supporting Information

The following file is available free of charge on the ACS Publications website at DOI: 10.1021/cs501345g.

XRD patterns, SEM images, ammonia-TPD profiles, N_2 adsorption and desorption isotherm of H-SSZ-13 zeolite, FT-IR spectra, mass of hydrocarbons retained in the catalyst material for different reaction temperatures at a WHSV value of 0.5 g g^{-1} h^{-1}, operando UV−vis spectra of H-SSZ-13 collected at the beginning of the MTO reaction, and deconvolution of the operando UV−vis spectra of H-SSZ-13 into two groups of absorption bands (eigenspectra) for the MTO reaction at 598, 623, 648, and 673 K (PDF)

■ AUTHOR INFORMATION

Corresponding Authors

*J.R.-M.: e-mail, j.ruizmartinez@uu.nl; tel, +31 62 273 6379.
*B.M.W.: e-mail, b.m.weckhuysen@uu.nl; tel, +31 30 253 4328.

Notes

The authors declare no competing financial interest.

■ ACKNOWLEDGMENTS

This research work was funded by The Netherlands Research School Combination-Catalysis (NRSC-C) and the Deanship of Scientific Research (DSR) of King Abdulaziz University, Jeddah, Saudi Arabia, under grant number (T-002-431). J.R.-M. (Utrecht University, The Netherlands) also acknowledges the CW-NWO for his VENI grant. Sachem Inc. is acknowledged for providing the template for the synthesis of the H-SSZ-13 catalyst material. J. A. Stewart and P. Wijten, both of Utrecht University, are acknowledged for the assistance with GC-MS analysis of the retained hydrocarbons. S. Kalirai of Utrecht University is acknowledged for valuable discussions about NNMF analysis of UV−vis spectra.

■ REFERENCES

(1) Olsbye, U.; Svelle, S.; Bjørgen, M.; Beato, P.; Janssens, T. V. W.; Joensen, F.; Bordiga, S.; Lillerud, K. P. *Angew. Chem., Int. Ed.* **2012**, *51*, 5810−5831.
(2) Stoecker, M. *Microporous Mesoporous Mater.* **1999**, *29*, 3−48.
(3) Hunger, M. In *Zeolites and Catalysis, Synthesis, Reactions and Application*; Cejka, J., Corma, A., Zones, S., Eds.; Wiley-VCH: Weinheim, Germany, 2010; Vol. 2, p 493.
(4) Dessau, R. M. *J. Catal.* **1986**, *99*, 111−116.
(5) Bleken, F. L.; Janssens, T. V. W.; Svelle, S.; Olsbye, U. *Microporous Mesoporous Mater.* **2012**, *164*, 190−198.
(6) Dahl, I. M.; Kolboe, S. *Catal. Lett.* **1993**, *20*, 329−336.
(7) Yuen, L.-T.; Zones, S. I.; Harris, T. V.; Gallegos, E. J.; Auroux, A. *Microporous Mater.* **1994**, *2*, 105−117.
(8) Kumita, Y.; Gascon, J.; Stavitski, E.; Moulijn, J. A.; Kapteijn, F. *Appl. Catal. A: Gen.* **2011**, *391*, 234−243.
(9) Lok, B. M.; Messina, C. A.; Patton, R. L.; Gajek, R. T.; Cannan, T. R.; Flanigen, E. M. *J. Am. Chem. Soc.* **1984**, *106*, 6092−6093.
(10) Hereijgers, B. P. C.; Bleken, F.; Nilsen, M. H.; Svelle, S.; Lillerud, K.-P.; Bjørgen, M.; Weckhuysen, B. M.; Olsbye, U. *J. Catal.* **2009**, *264*, 77−87.
(11) Bleken, F.; Bjørgen, M.; Palumbo, L.; Bordiga, S.; Svelle, S.; Lillerud, K.-P.; Olsbye, U. *Top. Catal.* **2009**, *52*, 218−228.
(12) Dai, W.; Wu, G.; Li, L.; Guan, N.; Hunger, M. *ACS Catal.* **2013**, *3*, 588−596.
(13) Aramburo, L. R.; Ruiz-Martínez, J.; Sommer, L.; Arstad, B.; Buitrago-Sierra, R.; Sepúlveda-Escribano, A.; Zandbergen, H. W.; Olsbye, U.; de Groot, F. M. F.; Weckhuysen, B. M. *ChemCatChem* **2013**, *5*, 1386−1394.
(14) Hunger, M. *Microporous Mesoporous Mater.* **2005**, *82*, 241−255.
(15) Dai, W.; Wang, X.; Wu, G.; Guan, N.; Hunger, M.; Li, L. *ACS Catal.* **2011**, *1*, 292−299.
(16) Park, J. W.; Seo, G. *Appl. Catal. A: Gen.* **2009**, *356*, 180−188.
(17) Mores, D.; Stavitski, E.; Kox, M. H. F.; Kornatowski, J.; Olsbye, U.; Weckhuysen, B. M. *Chem. Eur. J.* **2008**, *14*, 11320−11327.
(18) Mores, D.; Kornatowski, J.; Olsbye, U.; Weckhuysen, B. M. *Chem. Eur. J.* **2011**, *17*, 2874−2884.
(19) Qian, Q.; Ruiz-Martínez, J.; Mokhtar, M.; Asiri, A. M.; Al-Thabaiti, S. A.; Basahel, S. N.; van der Bij, H. E.; Kornatowski, J.; Weckhuysen, B. M. *Chem. Eur. J.* **2013**, *19*, 11204−11215.
(20) Li, J.; Xiong, G.; Feng, Z.; Liu, Z.; Xin, Q.; Li, C. *Microporous Mesoporous Mater.* **2000**, *39*, 275−280.
(21) Wragg, D. S.; Johnsen, R. E.; Balasundaram, M.; Norby, P.; Fjellvåg, H.; Grønvold, A.; Fuglerud, T.; Hafizovic, J.; Vistad, Ø. B.; Akporiaye, D. *J. Catal.* **2009**, *268*, 290−296.
(22) Arstad, B.; Kolboe, S. *J. Am. Chem. Soc.* **2001**, *123*, 8137−8138.

DOI: 10.1021/cs501345g
ACS Catal. 2015, 5, 992−1003

(23) Dahl, I. M.; Kolboe, S. *J. Catal.* **1994**, *149*, 458−464.
(24) McCann, D. M.; Lesthaeghe, D.; Kletnieks, P. W.; Guenther, D. R.; Hayman, M. J.; Van Speybroeck, V.; Waroquier, M.; Haw, J. F. *Angew. Chem., Int. Ed.* **2008**, *47*, 5179−5182.
(25) Haw, J. F.; Song, W.; Marcus, D. M.; Nicholas, J. B. *Acc. Chem. Res.* **2003**, *36*, 317−326.
(26) Wu, L.; Degirmenci, V.; Magusin, P. C. M. M.; Szyja, B. M.; Hensen, E. J. M. *Chem. Commun.* **2012**, *48*, 9492−9494.
(27) Wu, L.; Degirmenci, V.; Magusin, P. C. M. M.; Lousberg, N. J. H. G. M.; Hensen, E. J. M. *J. Catal.* **2013**, *298*, 27−40.
(28) Moliner, M.; Franch, C.; Palomares, E.; Grill, M.; Corma, A. *Chem. Commun.* **2012**, *48*, 8264−8266.
(29) Lee, D. D.; Seung, H. S. *Nature* **1999**, *401*, 788−791.
(30) Lee, D. D.; Seung, H. S. In *Advances in Neural Information Processing Systems 13*; Proceedings of the 2000 Conference, Vancouver, Canada, Dec 3−8, 2001; Leen, T. K., Dietterich, T. G., Tresp, V., Eds.; Massachusetts Institute of Technology: Cambridge, MA, 2001; pp 556−562.
(31) Berry, M. W.; Browne, M.; Langville, A. N.; Pauca, V. P.; Plemmons, R. J. *Comput. Stat. Data Anal.* **2007**, *52*, 155−173.
(32) Lezcano-Gonzalez, I.; Deka, U.; Arstad, B.; Van Yperen-De Deyne, A.; Hemelsoet, K.; Waroquier, M.; Van Speybroeck, V.; Weckhuysen, B. M.; Beale, A. M. *Phys. Chem. Chem. Phys.* **2014**, *16*, 1639−1650.
(33) Jeon, H.-Y.; Shin, C.-H.; Jung, H. J.; Hong, S. B. *Appl. Catal. A: Gen.* **2006**, *305*, 70−78.
(34) Bordiga, S.; Regli, L.; Cocina, D.; Lamberti, C.; Bjørgen, M.; Lillerud, K. P. *J. Phys. Chem. B* **2005**, *109*, 2779−2784.
(35) Froment, G. F.; Dehertog, W. J. H.; Marchi, A. J. In *Catalysis*; Spivey, J. J., Ed.; Royal Society of Chemistry: London, 1992; Vol. *9*, p 9.
(36) Marchi, A. J.; Froment, G. F. *Appl. Catal.* **1991**, *71*, 139−152.
(37) Feller, A.; Guzman, A.; Zuazo, I.; Lercher, J. A. *J. Catal.* **2004**, *224*, 80−93.
(38) Marcus, D. M.; McLachlan, K. A.; Wildman, M. A.; Ehresmann, J. O.; Kletnieks, P. W.; Haw, J. F. *Angew. Chem., Int. Ed.* **2006**, *45*, 3133−3136.
(39) Zhu, Q.; Kondo, J. N.; Tatsumi, T.; Inagaki, S.; Ohnuma, R.; Kubota, Y.; Shimodaira, Y.; Kobayashi, H.; Domen, K. *J. Phys. Chem. C* **2007**, *111*, 5409−5415.
(40) Kiricsi, I.; Förster, H.; Tasi, G.; Nagy, J. B. *Chem. Rev.* **1999**, *99*, 2085−2114.
(41) Wulfers, M. J.; Jentoft, F. C. *J. Catal.* **2013**, *307*, 204−213.
(42) Haw, J. F.; Nicholas, J. B.; Song, W.; Deng, F.; Wang, Z.; Xu, T.; Heneghan, C. S. *J. Am. Chem. Soc.* **2000**, *122*, 4763−4775.
(43) Bjørgen, M.; Bonino, F.; Kolboe, S.; Lillerud, K.-P.; Zecchina, A.; Bordiga, S. *J. Am. Chem. Soc.* **2003**, *125*, 15863−15868.
(44) Bjørgen, M.; Bonino, F.; Arstad, B.; Kolboe, S.; Lillerud, K.-P.; Zecchina, A.; Bordiga, S. *ChemPhysChem* **2005**, *6*, 232−235.
(45) Van Speybroeck, V.; Hemelsoet, K.; De Wispelaere, K.; Qian, Q.; Van der Mynsbrugge, J.; De Sterck, B.; Weckhuysen, B. M.; Waroquier, M. *ChemCatChem* **2013**, *5*, 173−184.
(46) Hemelsoet, K.; Qian, Q.; De Meyer, T.; De Wispelaere, K.; De Sterck, B.; Weckhuysen, B. M.; Waroquier, M.; Van Speybroeck, V. *Chem. Eur. J.* **2013**, *19*, 16595−16606.
(47) Song, W.; Haw, J. F.; Nicholas, J. B.; Heneghan, C. S. *J. Am. Chem. Soc.* **2000**, *122*, 10726−10727.
(48) Arstad, B.; Kolboe, S. *Catal. Lett.* **2001**, *71*, 209−212.
(49) Haw, J. F.; Marcus, D. M. *Top. Catal.* **2005**, *34*, 41−48.
(50) Song, W.; Marcus, D. M.; Fu, H.; Ehresmann, J. O.; Haw, J. F. *J. Am. Chem. Soc.* **2002**, *124*, 3844−3845.
(51) Dai, W.; Scheibe, M.; Guan, N.; Li, L.; Hunger, M. *ChemCatChem.* **2011**, *3*, 1130−1133.
(52) Park, J. W.; Lee, J. Y.; Kim, K. S.; Hong, S. B.; Seo, G. *Appl. Catal. A: Gen.* **2008**, *339*, 36−44.
(53) Dai, W.; Scheibe, M.; Li, L.; Guan, N.; Hunger, M. *J. Phys. Chem. C* **2012**, *116*, 2469−2476.
(54) Palumbo, L.; Bonino, F.; Beato, P.; Bjørgen, M.; Zecchina, A.; Bordiga, S. *J. Phys. Chem. C* **2008**, *112*, 9710−9716.
(55) Kiricsi, I.; Förster, H. *J. Chem. Soc. Faraday Trans. 1* **1988**, *84*, 491−499.
(56) Demidov, A. V.; Davydov, A. A. *Mater. Chem. Phys.* **1994**, *39*, 13−20.

DOI: 10.1021/cs501345g
ACS Catal. 2015, 5, 992−1003